Penetrant transport in semicrystalline poly(ethylene terephthalate)

G. F. Billovits and C. J. Durning*
Department of Chemical Engineering and Applied Chemistry, Columbia University, New York, NY 10027, USA
(Received 20 August 1987; revised 9 March 1988; accepted 9 March 1988)

This paper examines the unsteady transport of liquid methanol, acetone, and dimethylformamide (DMF) in thin films of unoriented, semicrystalline poly(ethylene terephthalate) (PET). Three different semicrystalline fine structures were prepared; one by solvent induced crystallization (SINC) and two by thermal annealing procedures. Penetrant mass uptake and sample dimensional changes were followed during integral sorption experiments at temperatures in the range 25–75°C. Optical cross-sections of partially swollen films and penetrant desorption from equilibrated films were also studied. For films prepared by thermal annealing, the methanol transport is classical, while in SINC films, the process shows some non-classical (non-Fickian) characteristics. For both acetone and DMF, the transport is non-Fickian; the non-Fickian effects are consistent with current phenomenological models. The influence of semicrystalline fine structure on the transport is subtle for methanol, but very strong for acetone and DMF. The profound effect on the non-Fickian transport results from the significant influence of fine structure on the polymer's mechanical properties. The appearance of non-Fickian behaviour is successfully predicted by an appropriate Deborah number correlation.

(Keywords: poly(ethylene terephthalate); semicrystalline; non-Fickian transport; diffusion Deborah number)

INTRODUCTION

The unsteady transport of small penetrants in high polymers has been studied for many years; the observed behaviours range from ordinary, classical diffusion to complicated, non-classical transport. The latter is not completely understood.

One can separate unsteady penetrant transport processes into two classes according to the magnitude of the concentration interval, i.e., according to the difference between characteristic initial and final penetrant concentrations. When the interval is small enough that material properties remain practically constant, the process can be called *linear* because a mathematical representation is a linear initial value problem. When the interval is large enough so that concentration-dependent material properties vary significantly with time and position, the process can be called *non-linear* since its representation is a non-linear initial value problem. The diversity of transport behaviours reported reflects that non-linearities can complicate the dynamics.

In 1975, Vrentas *et al.*[1] proposed an empirical method to predict the type of behaviour in the linear case: the transport should be classical (i.e. Fickian) if the value of the diffusion Deborah number, $(DEB)_D$†, is either very large or very small; non-classical (i.e. non-Fickian) transport should appear when $(DEB)_D \simeq O(1)$. Predictions based on $(DEB)_D$ have been verified in a few cases[1-5], but a broad application of the idea has not been forthcoming for two reasons. First, $(DEB)_D$ is usually a strong function of concentration and varies considerably in typical applications while the Vrentas and Duda correlation applies only for linear processes. Second, as defined by Vrentas *et al.*[1], $(DEB)_D$ can be calculated only for viscoelastic liquids; it cannot characterize penetrant transport in solids such as crosslinked and semicrystalline polymers.

In this work, we investigated the non-linear, unsteady transport of a weak swelling agent, liquid methanol, and two strong swelling agents, liquid acetone and dimethylformamide (DMF), in unoriented, semicrystalline poly(ethylene terephthalate) (PET). The data show the influence of temperature and polymer crystalline fine structure on the transport. The Vrentas–Duda Deborah number correlation is modified and applied to predict the appearance of non-Fickian behaviour.

CHARACTERIZATION OF PENETRANT TRANSPORT

The current ability to predict non-Fickian transport kinetics quantitatively is limited. Some progress has been made towards a theory for linear transport[5,6] but a predictive formulation for the non-linear problem is still far away. Only a phenomenological understanding of non-linear effects exists through experiments and models. The latter emphasize the importance of coupling between diffusion and polymer deformation in determining the overall character of the transport.

As described by Alfrey *et al.*[7], non-linear, unsteady penetrant transport almost always falls between the two limits of classical and 'Case II'. Each limit corresponds to a distinct dynamic behaviour in a sorption/desorption experiment. For example, if the initial penetrant mass uptake during sorption, M_t, is represented as a function of

* To whom correspondence should be addressed
† For nomenclature see Appendix A

0032-3861/88/081468-17$03.00

time, t, by

$$M_t = Kt^n \tag{1}$$

where K and n are constants, then the limit $n=1/2$ is classical behaviour; the other limit, $n=1$, is Case II transport. Fujita[8] gives a comprehensive discussion of behaviours in sorption/desorption experiments corresponding to classical, Fickian diffusion along with commonly observed non-Fickian effects.

The ability to predict both classical and Case II limits is a requirement of a good model for non-linear transport. For subsequent discussions, we summarize two useful phenomenological models having this capability: the Astarita and Sarti[9] model and the Thomas and Windle[10] model.

Astarita and Sarti model

Astarita and Sarti[9] (A&S) assume a priori that a sharp boundary separates an outer swollen region from an unpenetrated glassy core. They assume ordinary, ideal diffusion in the swollen region between the sample surface and the boundary and neglect penetrant diffusion in the glassy core ahead of the boundary. The boundary moves with a velocity, U, controlled by unspecified processes in its immediate neighbourhood (A&S called these 'swelling'). U is specified in terms of the composition at the boundary to represent the influence of swelling kinetics on the overall transport.

When their model is analysed, the following characteristics emerge. In a semi-infinite slab, swelling controls the transport initially and Case II behaviour is observed: both the mass of penetrant absorbed and the position of the moving boundary increase linearly with time. This continues until the diffusional resistance in the swollen region becomes significant. Then, diffusion of penetrant from the film surface to the moving boundary becomes rate determining and Fickian-like behaviour is observed: both the weight uptake and the position of the boundary increase linearly with $t^{1/2}$.

The model predicts three possibilities for sorption in polymer films:

(1) in thin films, an appreciable concentration gradient never forms behind the boundary and Case II behaviour is observed;

(2) in films of intermediate thickness, Case II behaviour is exhibited initially but asymptotes to Fickian-like behaviour near the end of the process producing anomalous, sigmoid-shaped weight uptake curves;

(3) in thick films, the initial region of Case II behaviour is very short and Fickian-like behaviour dominates the process. The A&S[9] model therefore provides a simple mechanistic explanation for the generalizations enunciated by Alfrey *et al.*[7].

A number of extensions to the basic model have been published which broaden its capabilities: Astarita and Joshi[11] included the effects of penetrant diffusion in the glassy region. Sarti[12] included a more detailed rate law for U through the influence of an osmotic stress at the boundary; application of the model to desorption was done by Joshi and Astarita[13]; Gostoli and Sarti[14] incorporated the effects of mechanical stresses. *In toto*, the A&S model provides a very flexible description of non-linear, non-Fickian transport.

Thomas and Windle model

Thomas and Windle[10] (T&W) provide a more detailed treatment of the coupling between diffusive transport and 'swelling' without introducing a moving boundary formalism. They represent the penetrant flux, J_1, by Gibbs' relation[15]

$$J_1 = \frac{-D_T(\phi_1)}{RT}\phi_1 \frac{d\mu_1}{dz} \tag{2}$$

where $D_T(\phi_1)$ is the thermodynamic diffusion coefficient, and ϕ_1 is the local penetrant concentration. The relationship

$$\frac{\mu_1 - \mu_1^0}{RT} = \ln \phi_1 + \frac{\pi V_1}{RT} \tag{3}$$

was proposed for the local penetrant chemical potential, μ_1. Here, V_1 is the molar volume of the penetrant, R is the gas constant, and T is temperature. One can show that π is equivalent to a mechanical pressure driving the local dilation of the polymer 'matrix'[3].

T&W[10] represented π by a simple viscous constitutive relationship

$$\frac{\partial \phi_1}{\partial t} = \frac{\pi}{k\eta(\phi_1)} \tag{4}$$

where k is a constant and $\eta(\phi_1)$ is a composition-dependent viscosity. The plasticizing effect of the penetrant was represented by

$$\eta(\phi_1) = \eta_0 \exp(-m\phi_1) \tag{5}$$

where η_0 is the pure polymer viscosity and m is a constant. This leads to

$$\frac{\partial \phi_1}{\partial t} = \frac{\partial}{\partial z} D_T \frac{\partial \phi_1}{\partial z} + \frac{kV_1}{RT}\frac{\partial}{\partial z} D_T \phi_1 \frac{\partial}{\partial z}\eta \frac{\partial \phi_1}{\partial t} \tag{6}$$

as the unsteady penetrant mass balance.

T&W[10] solved equation (6) numerically with boundary and initial conditions appropriate for integral sorption. By estimating the physical properties and their concentration dependence, they were able to predict semi-quantitatively the concentration profiles and weight uptake kinetics observed[16] during integral sorption of liquid methanol in poly(methyl methacrylate) (PMMA) films in the range 0–62°C. Their predictions include all the essential features of the Case II behaviour observed at low temperatures as well as a tendency toward classical behaviour at higher temperatures.

The models of A&S[9] and T&W[10] are in fact conceptually similar although this is not clearly recognized in the literature. For the Case II process, the T&W[10] model predicts a boundary whose motion is controlled by creep of the nearly dry polymer in response to the 'swelling pressure', π, just ahead of the boundary. The A&S[9] model includes essentially the same information within the framework of a moving boundary model. This is made clear in refinements by Sarti[12], who developed a rate equation for U based on the kinetics of crazing of glassy polymer just ahead of the moving boundary in response to an osmotic stress at the boundary. Clearly, both the A&S[9] and T&W[10] models postulate that the mechanical response of the glass to a thermodynamically defined stress controls the boundary motion during Case II. When Fickian-like behaviour is predicted, the calculations of T&W[10] show that the local

creep process becomes quite rapid and the transport becomes diffusion controlled in the same way that the A&S[9] model rapidly approaches diffusion control if the moving boundary velocity, U, is large.

In our view, the two models are complementary; that of A&S[9] provides analytical asymptotic formulae and simple physical interpretations of the limiting behaviours. The model of T&W[10] gives a more detailed mechanistic understanding of the Case II limit, especially of the factors controlling the moving boundary velocity, but it must be handled numerically.

EXPERIMENTAL

Materials

Amorphous, unoriented sheets of PET (E.I. duPont Co.), 0.305 and 0.406 mm in thickness, were cut into strips 1.6 × 3.8 cm and crystallized by one of three procedures. The first involved 'solvent induced crystallization' (SINC) whereby the amorphous polymer was crystallized by the vapour of an interactive penetrant. Pre-weighed amorphous samples were exposed to saturated methylene chloride vapour at room temperature for 3 h. Durning *et al.*[17] showed that such treatment leads to uniformly crystalline material without the surface cavitation produced by liquid penetrants. After air drying at room temperature for 8 h, residual methylene chloride was leached from the films by immersion in methanol at 62°C for 24 h. The samples were then dried under high vacuum at 80°C for 48 h and then weighed to ensure they had returned to their initial, amorphous weight. Samples exhibiting a net weight increase were returned to the vacuum oven until the original weight was achieved.

The two other procedures involved crystallization by isothermal annealing, one (120°C) near the glass transition temperature (T_g) and the other (230°C) near the melting temperature. For both procedures, amorphous films were first heated under vacuum at 80°C for 24 h to relieve residual stresses and to nucleate crystallites. In the low temperature annealing (LTA) procedure, the samples were then crystallized by heating under vacuum at 120°C for 48 h. In the high temperature annealing (HTA) procedure, the vacuum oven was first flushed with dry nitrogen to prevent oxidation and then the samples were crystallized by heating under high vacuum at 230°C for 24 h. In all cases, the samples were slowly cooled to room temperature within the vacuum oven.

These crystallization procedures induce spherulitic morphologies with three different crystalline fine structures. Studies of these fine structures by X-ray and *FT*i.r. spectroscopy have been done by Dumbleton and Murayama[18], Makarewicz and Wilkes[19], and Lin and Koenig[20]. Their effects on the polymer mechanical properties and T_g were studied by Illers and Breuer[21], and Zachmann and Schermann[22] using dynamic mechanical methods. These works give a clear picture of the distinct semicrystalline morphologies achieved in each case and provide physical property data relevant to our analysis.

The SINC and LTA preparation of PET both lead to low overall levels of crystallinity; the crystalline volume fraction, α_c, is ~0.23 for the former and ~0.28 for the latter. In the case of SINC, crystallization proceeds from a swollen system giving imperfect lamellar crystallites (more precisely a small long spacing results) and amorphous domains with unrestricted or 'loose' tie molecules[20]. During the LTA procedure, crystallization takes place only slightly above T_g where the chain segments have limited mobility. Wide-angle X-ray[18] and *FT*i.r.[20] measurements indicate that imperfect lamellar crystallites again develop, but the remaining disordered phase contains stretched, taut tie molecules between crystallites.

Annealing glassy PET at high temperature (HTA procedure) leads to a high level of crystallinity ($\alpha_c \simeq 0.43$). Since crystallization takes place far above T_g, the chain segments possess a high degree of mobility during fusion so more perfect lamellae are produced (i.e. a large long spacing results). Segments unable to crystallize, such as entangled loops and tie chains between crystallites, are left unconstrained.

The differences among the three fine structures are reflected by their distinct mechanical properties. For all three morphologies, the peak in tan δ is spread over a larger time/temperature range than for the amorphous polymer. This broadening increases with increasing crystallinity (SINC < LTA < HTA) due to the greater spread in the distribution of amorphous chain lengths at higher levels of crystallinity. For each of the semicrystalline morphologies, the T_g is elevated significantly over the value for the amorphous polymer (~75°C) due to restrictions on the disordered chains by the crystallites. The glassy modulus, G_0, of the semicrystalline polymer is also increased. For both T_g and G_0, the increase is smaller for PET prepared by SINC than for the thermally annealed samples. Relevant physical data are shown in *Table 1*.

Density measurements

The crystalline volume fraction, α_c, for representative samples was determined prior to transport measurements from density (*Table 1*). Density measurements were made by the gradient method (ASTM standard D1505) using n-heptane and carbon tetrachloride as the immersion media. After transport experiments, representative samples were leached in methanol at 62°C for 24 h to remove residual penetrant and dried under vacuum at 80°C for 48 h. The density was then remeasured to determine whether additional crystallization had taken place during the transport experiments. In all cases, no significant additional crystallization ($\Delta\alpha_c < 0.02$) was detected.

Table 1 Physical parameters for semicrystalline PET films

Film preparation	ρ (23°C)[a]	Crystalline volume fraction, α_c[b]	T_g (°C)[c]
SINC	1.375	0.23	90
Low temperature annealing	1.382	0.27	107
High temperature annealing	1.411	0.43	102

[a] ASTM Standard D1505
[b] Calculated using $\alpha_c = (\rho - \rho_a)/(\rho_c - \rho_a)$ where $\rho_a = 1.335$, $\rho_c = 1.510$
[c] Determined from the dynamic mechanical data of Illers and Breuer[21] and Zachmann and Schermann[22]

Table 2 Summary of transport experiments[a]

Film preparation	Integral sorption	Integral desorption	Dimensional changes	Optical microscopy
Methanol				
SINC	45, 62	62	62	62
Low temperature annealing	35, 45, 55, 62	62	55, 62	62
High temperature annealing	62	—	62	—
DMF				
SINC	25, 45, 65, 75	65	45, 65, 75	65
Low temperature annealing	45, 65, 75	65	45, 65, 75	65
High temperature annealing	45, 65, 75	65	45, 65, 75	65
Acetone				
SINC	35, 45, 53	—	53	—
Low temperature annealing	35, 45, 53	—	53	—
High temperature annealing	35, 45, 53	—	—	—

[a] Experimental temperatures for each technique (°C)

Transport measurements

The penetrants employed were reagent grade methanol, acetone and DMF. These were used as received (Fisher) without purification. Constant temperature was maintained by a water bath and temperature controller (Yellow Springs Instruments Model 63 RC, accuracy ± 0.05°C). *Table 2* summarizes the conditions examined for each penetrant by each of the following experimental techniques.

Integral sorption. Integral sorptions were carried out using pure penetrant liquids and dry semicrystalline PET films. Weight uptake as a function of immersion time was followed by gravimetry on approximately 20 different samples. The films were removed periodically from the liquid, blotted dry, and weighed in a stoppered vial (Mettler balance, sensitivity ± 0.0001 g). For methanol sorption, only one measurement was made on each sample; for the other two penetrants, the films were returned to the penetrant liquid once or twice for further measurements. In all cases, the time during weighings was a negligible fraction of the total immersion time.

Dimensional change measurements. The thickness of a single sample was measured periodically using a dial gauge comparator (Standard, sensitivity ± 2.5 μm). Length (one dimension of the lateral area) was measured *in situ* using a cathetometer (Gaertner, sensitivity ± 1 μm) while the sample was held flat between wire screens in an optical cell containing the swelling agent.

Optical microscopy. In order to assess whether transport was accompanied by a moving boundary, film samples were immersed in the liquid, removed before equilibrium, sectioned, and examined by optical microscopy. To make a sharp front readily visible, the penetrant was coloured by a small addition of iodine (4 g/100 ml penetrant). Cross-sections, approximately 8 μm thick, were microtomed (American Optical Model 820) from samples immediately upon removal from the penetrant. The sections were then fixed on a microscope slide and refrigerated ($T < 0$°C) for later viewing in an optical microscope. With iodine as a stain, the position of a penetrant diffusion front was readily seen.

Desorption. Integral desorption from fully swollen films was studied. Samples were allowed to equilibrate with the liquid penetrant at the desired temperature. They were then transferred to an evacuated tube maintained at constant temperature. The samples were periodically removed, weighed (Mettler balance, sensitivity ± 0.0001 g), and returned to the evacuated tube for further desorption.

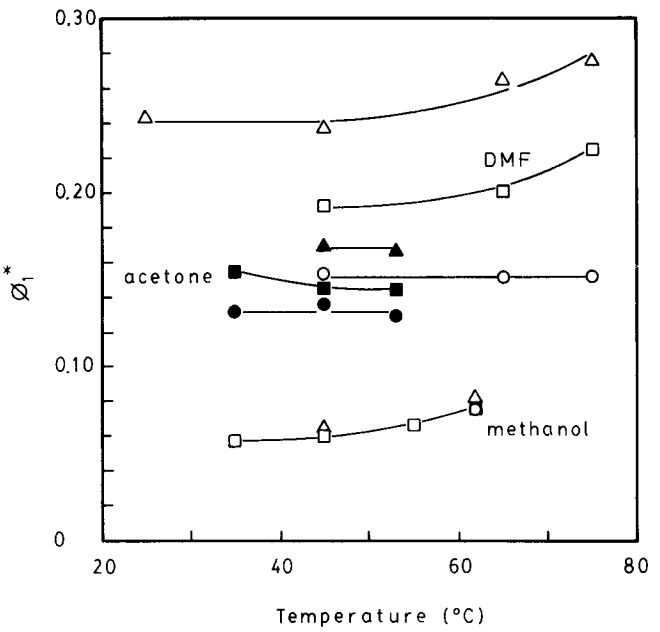

Figure 1 Equilibrium penetrant volume fraction in the amorphous phase, ϕ_1^*, *versus* temperature for PET prepared by SINC (△), LTA (□) and HTA (○). Open symbols (top) indicate DMF data; filled symbols (middle) indicate acetone data; open symbols (bottom) indicate methanol data

RESULTS AND DISCUSSION

Concentration interval

The concentration interval determines whether the transport is linear, i.e. whether the physical properties governing the transport vary significantly during the process. Since the films were initially dry, the interval is characterized by the penetrant's solubility in the polymer. We report the solubility based on the amorphous volume deduced from the crystalline volume fractions reported in *Table 1*.

Figure 1 shows the equilibrium penetrant volume fraction in the amorphous phase, ϕ_1^*, as a function of temperature for each penetrant in films prepared by the three procedures. For a given morphology, the solubility

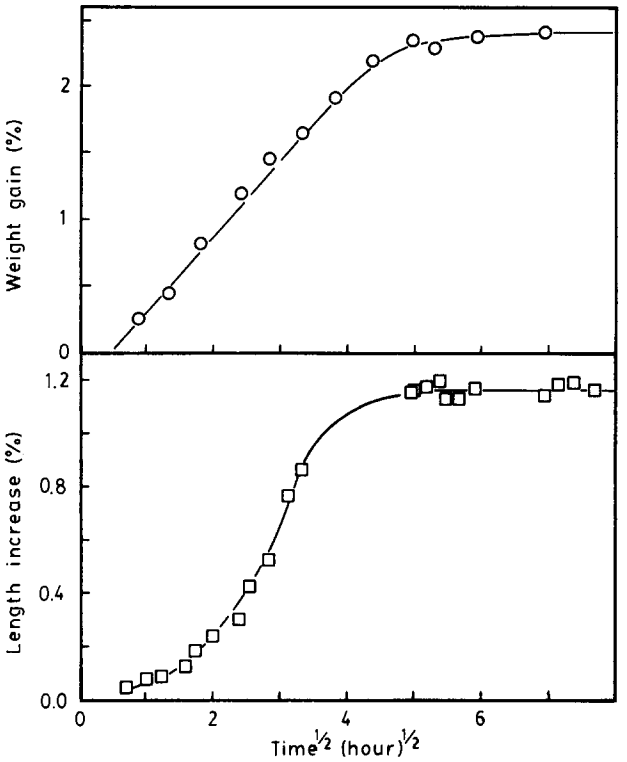

Figure 2 Weight gain and sample dimensional change data *versus* $t^{1/2}$ during methanol sorption at 62°C in films prepared by HTA

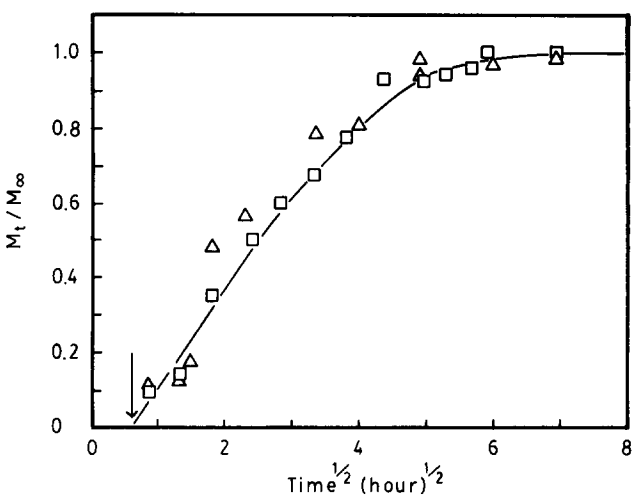

Figure 3 Relative weight uptake, M_t/M_∞, *versus* $t^{1/2}$ during methanol sorption at 62°C in films prepared by LTA (△) and HTA (□). Arrow points to apparent induction time

follows: DMF > acetone > methanol, which indicates the relative 'strength' of each penetrant as a swelling agent. For DMF in films prepared by HTA and for acetone in all morphologies, the solubility remains constant within experimental error. For both methanol and the remaining DMF cases, the solubility clearly increases with temperature indicating a positive enthalpy of dilution[23]: $\sim +9$ kJ mol^{-1} for methanol, $\sim +3$ kJ mol^{-1} for DMF.

The effect of morphology on the solubility depends on the strength of the swelling agent. For methanol, no change occurs with morphology; hence, any differences in transport behaviour are not explicable solely on the basis of non-linearities introduced by the concentration dependence of transport properties. In fact, we show subsequently that the concentration interval corresponding to ϕ_1^* for methanol introduces only weak non-linearities.

For acetone, a moderate trend with morphology is observed, while for DMF, the trend is relatively large. In both cases, ϕ_1^* follows: SINC > LTA > HTA, which parallels the trend in amorphicity $(1-\alpha_c)$. The connection between ϕ_1^* and $(1-\alpha_c)$ is clear if one draws an analogy between a semicrystalline system and a network. The crystallites act like network junctions so a highly crystalline sample behaves like a network with a high junction density. It follows that a strong swelling agent will have a lower ϕ_1^* in samples with higher crystallinity due to the larger entropic penalty associated with dilation of the 'network'. The difference is not seen for the weak swelling agent, methanol, since the entropic penalty is always minor.

Methanol transport

Effect of morphology. *Figure 2* shows the weight gain and length change data for methanol at 62°C in PET films prepared by HTA; the sorption was essentially identical for films prepared by LTA (*Figure 3*). In both cases, the transport appears to be classical: weight gain increases linearly with $t^{1/2}$ and is accompanied by isotropic dimensional changes. The short induction time in the weight gain curves (arrow in *Figure 3*) is not statistically significant; this is discussed in greater detail later. Microtomed sections of the thermally annealed films partially swollen in a methanol/iodine mixture show diffuse concentration profiles lacking any sharp fronts (*Figure 4*) as expected for classical transport with a nearly constant diffusion coefficient.

The desorption data give further evidence that the methanol transport is classical in the thermally crystallized samples. *Figure 5* shows desorption data from LTA films at 62°C plotted as relative weight loss $(1-M_t/M_\infty)$ vs. $t^{1/2}$. The dotted lines show the corresponding sorption data both with and without the apparent induction time. As in the plot for sorption, the weight of solvent desorbed vs. $t^{1/2}$ is initially linear, but grows increasingly concave to the abscissa. When the induction time is removed, the curve for desorption lies

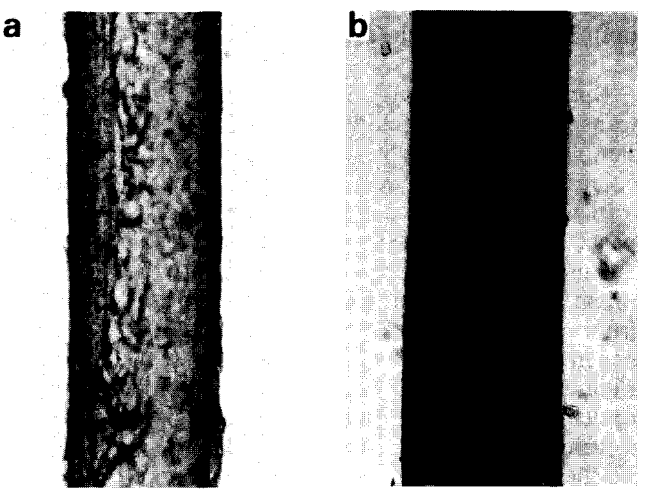

Figure 4 Representative optical micrographs of films prepared by LTA partially swollen with methanol at 62°C. Immersion time: (a) 1.0 h, (b) 13.4 h

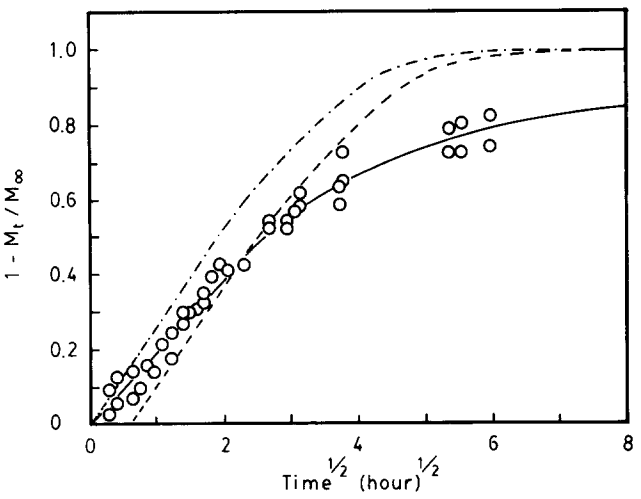

Figure 5 Desorption data at 62°C from films prepared by LTA and swollen to equilibrium with methanol, plotted as $(1-M_t/M_\infty)$ *versus* $t^{1/2}$. ----, Corresponding sorption data with the apparent induction time; –·–·, sorption data with the apparent induction time removed

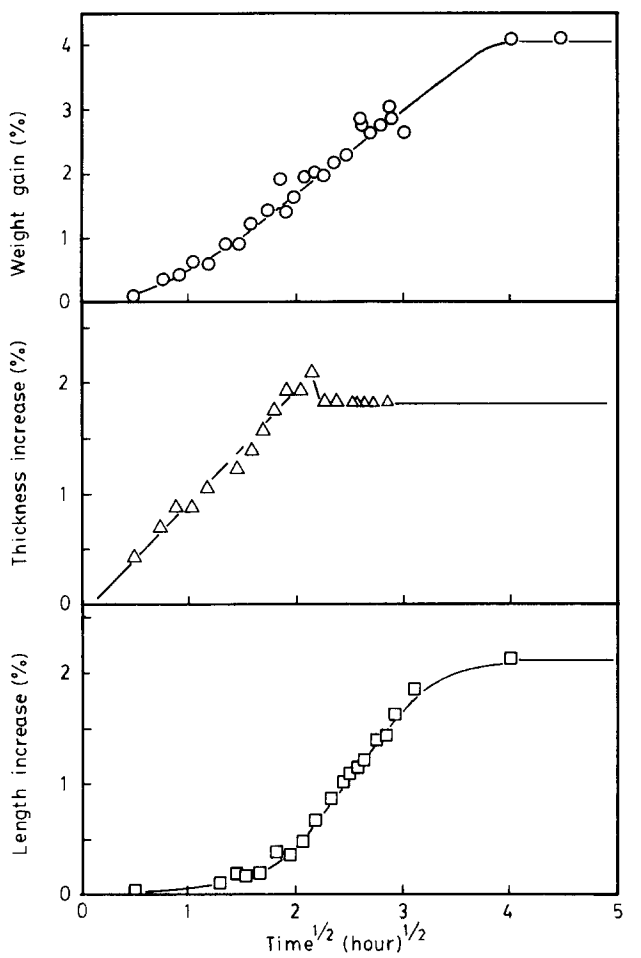

Figure 6 Weight gain and sample dimensional change data *versus* $t^{1/2}$ during methanol sorption at 62°C in films prepared by SINC

entirely below that for sorption, a result characteristic of classical, Fickian diffusion with a diffusion coefficient increasing with concentration[8]. If the apparent induction time is not removed, the sorption and desorption curves are approximately coincident initially, but the desorption curve grows concave to the axis more quickly; this behaviour is characteristic of Fickian diffusion with a concentration-independent diffusion coefficient[8].

Fujita[8] summarized other characteristics of classical transport which were not tested. For example, in our experiments only one sample thickness was used, so the superposition of sorption/desorption data for different thicknesses was not tested. Nevertheless, the present data are largely consistent with classical transport characterized by a diffusion coefficient either increasing or constant with penetrant concentration.

By contrast, methanol sorption in PET prepared by SINC shows non-classical features. *Figure 6* shows the weight gain and sample dimensional change data *versus* $t^{1/2}$ for methanol sorption at 62°C in PET prepared by SINC. The weight gain curve is predominantly linear with $t^{1/2}$, but upward curvature is unmistakable at short times. This initial feature grows more obvious at lower temperatures, which is consistent with the phenomenological models for non-classical transport[9,10].

The dimensional change data for this case (*Figure 6*) show evidence of anisotropic swelling: the thickness change curve increases linearly with $t^{1/2}$, and passes through a maximum before achieving the equilibrium value; the length remains practically constant until the maximum in the thickness, after which, the length increases rapidly. This anisotropic swelling is typically found during non-Fickian transport[24] where a sharp boundary separates a swollen outer region from an unpenetrated, glassy core. The microtomed cross-sections (*Figure 7*) show a much steeper methanol gradient than in thermally annealed films reminiscent of the sharp moving boundaries during non-Fickian transport.

Further, the corresponding desorption data in *Figure 8* lie above the curve for sorption in contrast to the behaviour observed for the thermally annealed films. An initial rate of desorption greater than for sorption is a typical feature of non-Fickian transport and is never seen for classical diffusion[8]. Taken together, the data show a clear deviation from the classical predictions for methanol transport in PET prepared by SINC.

The data show that the characteristics of methanol transport in semicrystalline PET depend on the fine structure. We believe the effect results from the differences in the viscoelastic mechanical properties of the polymer induced by the different crystallization procedures. This

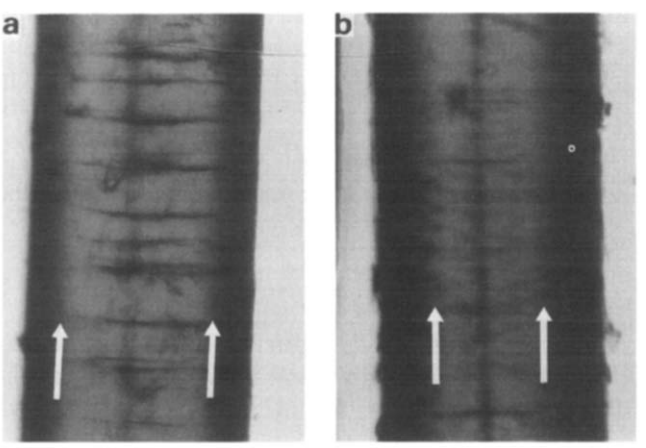

Figure 7 Representative optical micrographs of films prepared by SINC partially swollen with methanol at 62°C. Immersion time: (a) 4.0 h, (b) 7.1 h. Arrows show sharp concentration boundary

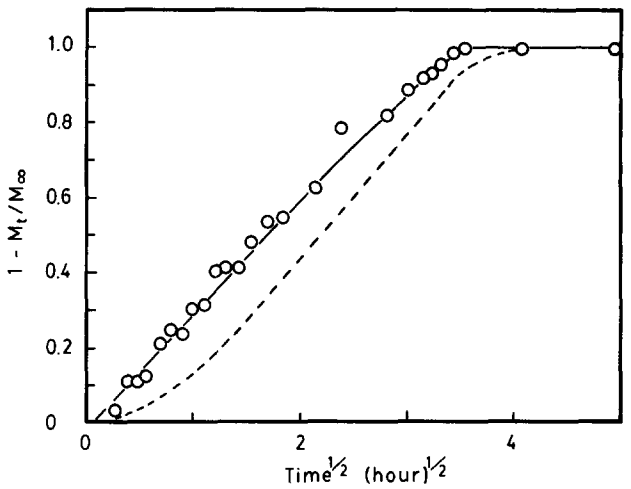

Figure 8 Desorption data at 62°C from films prepared by SINC and swollen to equilibrium with methanol, plotted as $(1-M_t/M_\infty)$ *versus* $t^{1/2}$. ----, Corresponding sorption data

Table 3 Diffusion coefficients ($cm^2\ s^{-1}$) calculated from methanol sorption data in thermally annealed PET films assuming classical behaviour

Temperature (°C)	Low temperature annealing	High temperature annealing
35	4.2×10^{-11}	—
45	1.1×10^{-10}	—
55	4.6×10^{-10}	—
62	6.3×10^{-10}	7.5×10^{-10}

Table 4 Diffusion coefficients calculated from methanol desorption data at 62°C assuming classical, concentration independent behaviour

Film preparation	D ($cm^2\ s^{-1}$)
SINC	4×10^{-9a}
Low temperature annealing	1×10^{-9}
High temperature annealing	—

[a] Approximated assuming classical behaviour although sorption was non-classical

notion is supported by calculations of the diffusion Deborah number presented later.

Weak non-linearities. As discussed above, methanol transport in thermally annealed films was classical. In order to assess the severity of the concentration dependence of the diffusion coefficient, i.e. of the non-linearity in the transport, diffusion coefficients calculated from sorption and desorption data were compared. Diffusion coefficients were obtained from the half times for sorption[25], neglecting the apparent induction period (see below), and assuming a diffusion coefficient independent of composition:

$$D=\frac{0.04919L^2}{t_{1/2}} \qquad (7)$$

Here D is the polymer fixed frame diffusion coefficient, L is the film half-thickness, and $t_{1/2}$ the time for which $M_t/M_\infty=0.5$. Values of D are reported in *Table 3*.

A corresponding diffusion coefficient was calculated from the initial rate of desorption at 62°C using the method of Crank and Park[25] (eq. (7)) again assuming concentration independence. The value from desorption was $1\times10^{-9}\ cm^2\ s^{-1}$ (*Table 4*); for sorption at the same conditions, the value was $6\times10^{-10}\ cm^2\ s^{-1}$ (*Table 3*). Clearly, for methanol in PET prepared by LTA, the transport is classical with a diffusivity only slightly increasing with concentration, i.e. with a weak non-linearity.

Although desorption experiments were not done for HTA films, it is likely that the non-linearities are also weak in this case since the concentration interval is the same. A similar comment applies for the non-classical transport in films prepared by SINC.

Effect of temperature. *Figures 9* and *10* show the effects of temperature on the methanol weight uptake in films prepared by LTA and SINC, respectively, the former being representative of behaviour in HTA films also. No dramatic changes are evident in the character of transport with temperature; only an increase in the rate of each process accompanies increased temperature.

For sorption in the thermally annealed PET, an

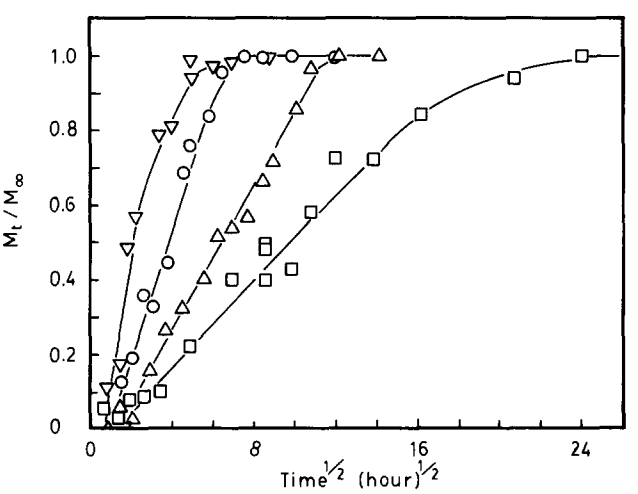

Figure 9 Relative weight uptake, M_t/M_∞, *versus* $t^{1/2}$ during methanol sorption in films prepared by LTA at 35°C (□), 45°C (△), 55°C (○) and 62°C (▽)

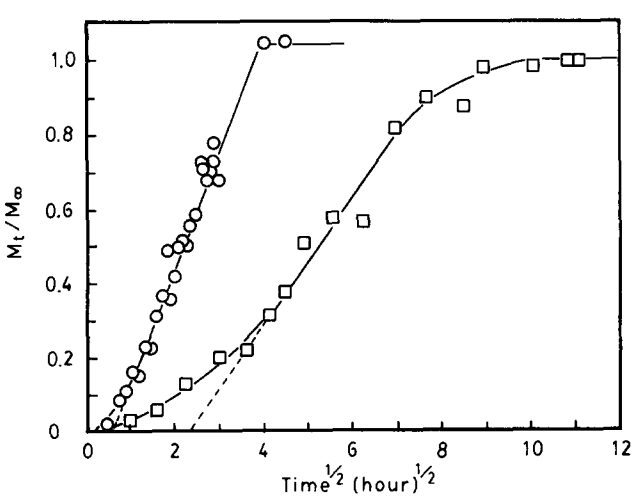

Figure 10 Relative weight uptake, M_t/M_∞, *versus* $t^{1/2}$ during methanol sorption in films prepared by SINC at 45°C (□) and 62°C (○). Extrapolations of the linear portion of the data give the induction times

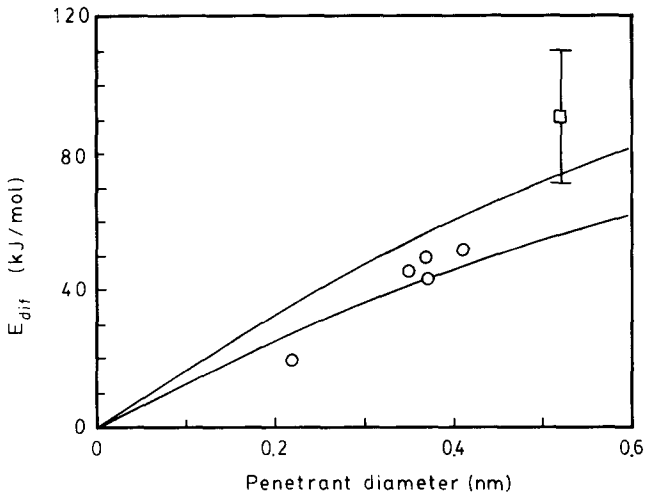

Figure 11 Activation energy for diffusion (kJ mol^{-1}) predicted by the theory of Pace and Datyner[27] *versus* penetrant diameter (nm) for semicrystalline PET below T_g using a local bending modulus (lower curve) and an average bending modulus (upper curve). Methanol data with error bars for films prepared by LTA (□). Data of Michaels *et al.*[26] (○)

Arrhenius analysis of D yields an activation energy of $+91 \pm 19$ kJ mol^{-1}. This falls in line with values found by Michaels *et al.*[26] for fixed gases in glassy, semicrystalline PET when interpreted by the molecular mechanics theory of Pace and Datyner[27]. The theory relates the apparent activation energy for diffusion with the polymer cohesive energy density, the polymer chain bending modulus and the molecular diameter of the penetrant. *Figure 11* shows a plot of activation energy for diffusion, E_{dif}, *versus* penetrant diameter (nm) for diffusion in semicrystalline PET below T_g according to Pace and Datyner's theory along with the data of Michaels *et al.*[26] and our data for methanol. The lower curve shows the predicted behaviour using a local chain bending modulus based on the rotational potentials of flexible glycol segments in the PET repeat unit, while the upper curve gives the prediction using a modulus averaged over several repeat units. Pace and Datyner[27] argue that the lower curve is applicable for smaller penetrants (He, H_2, O_2) while the upper curve is applicable for larger ones which require flexure of the chain over a larger portion of the backbone. The prediction based on the larger average bending modulus is within the uncertainty in the methanol data.

Induction time. We stated earlier that the weight uptake curves for methanol in thermally annealed films show an apparent induction time which is an artifact. This is made clear by comparing the effect of temperature on the classical diffusion in *Figure 9* with its effect on the non-Fickian transport in *Figure 10*. As explained in a subsequent section, an induction time usually accompanies non-Fickian transport; typically, this feature depends very strongly on temperature. This can be seen for methanol transport in SINC films by the extrapolations in *Figure 10*. By contrast, no induction time should appear in classical diffusion. We find no systematic effect of temperature on the apparent induction times in *Figure 9*. In addition, the magnitude of these induction times were within the uncertainty of an $M_t = 0$ intercept calculated from a least squares extrapolation of the linear portion of the curves. Consequently, we believe that the apparent induction times in *Figure 9* are artifacts of the gravimetric technique.

Acetone and DMF transport

First, we discuss representative data to show the general character of the transport for acetone and DMF. Typical weight gain and dimensional change data are juxtaposed in *Figures 12*, *13* and *14*; representative optical micrographs and the data taken therefrom appear in *Figures 15* and *16*.

DMF transport. *Figure 12* shows the sorption at 65°C of the strongest swelling agent, DMF, in PET prepared by SINC; the data are representative of all PET samples and over the entire temperature range examined. The transport is clearly non-classical.

The dimensional change curves show an extreme anisotropic swelling: the thickness increases linearly with $t^{1/2}$ initially, passes through a sharp maximum, then a minimum, and finally achieves the equilibrium value. The length increases only very slowly until the maximum in thickness; thereafter, it increases rapidly to the equilibrium value without an overshoot.

The corresponding weight gain plot is strikingly non-Fickian (*Figure 12*). After an induction time, the weight gain increases linearly with $t^{1/2}$ for a substantial period. Then, at a critical point, the weight gain ascends very

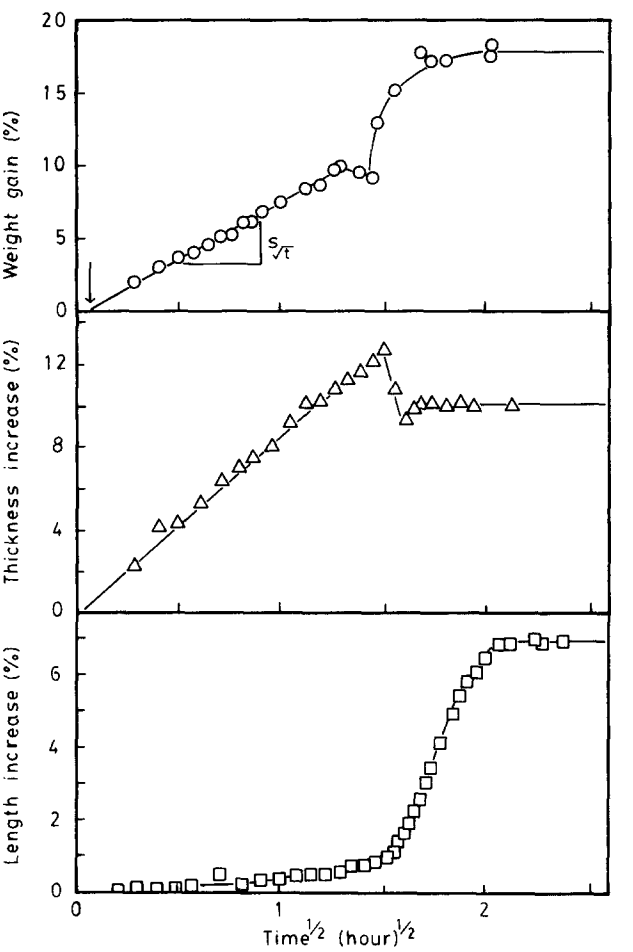

Figure 12 Weight gain and sample dimensional change data *versus* $t^{1/2}$ during DMF sorption at 65°C in films prepared by SINC. Arrow indicates the induction time; $s_{t^{1/2}}$ indicates the slope of the linear portion of the data

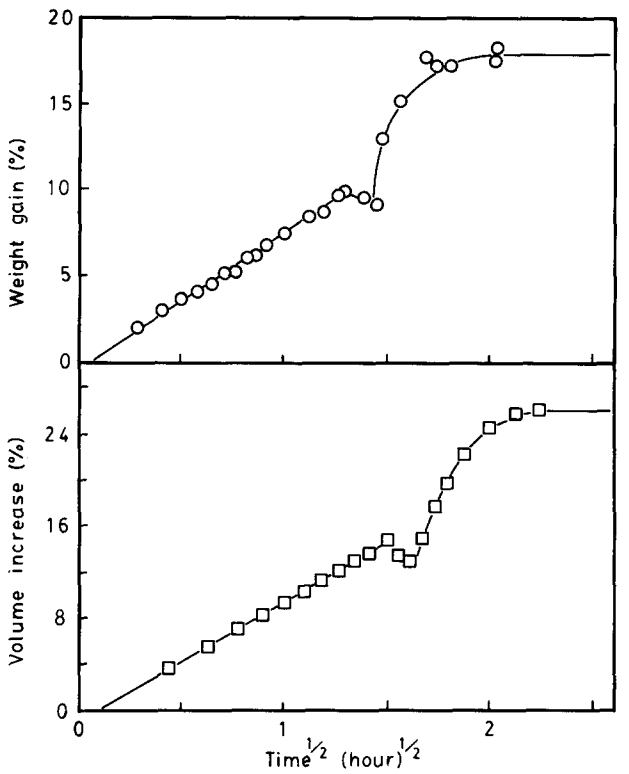

Figure 13 Juxtaposed plots of weight gain and volume change/original volume *versus* $t^{1/2}$ during DMF sorption at 65°C in films prepared by SINC

rapidly to the ultimate value in a manner resembling the 'Super Case II' transport reported by Jacques *et al.*[28]. For DMF sorption at 65°C in films prepared by SINC (*Figure 12*) we observed a shallow maximum before the rapid increase begins; for other combinations of morphology/temperature only the abrupt increase in the slope was observed. In every case, independent dimensional change data verified the weight gain curve: a plot of volume change/original volume *versus* $t^{1/2}$ could be prepared showing the same features as the weight gain curves (*Figure 13*).

From the juxtaposed plots (*Figure 12*), one sees that the maximum in thickness coincides with the beginning of rapid increases in weight gain and sample length. Evidently, the point of maximum thickness demarks the beginning of a dramatic shape rearrangement which accelerates the weight gain during the final stages of transport.

Using optical microscopy, the position of a penetrant diffusion front could be clearly observed. Microtomed cross-sections of films partially swollen in DMF coloured by iodine (4 g/100 ml) reveal very sharp moving boundaries accompanying the transport (*Figure 15*); these first become visible at the edges of the film after the induction time. The dramatic increase in the rate of weight uptake occurs as the boundaries approach the film centreline; this is consistent with the phenomenology of the 'Super Case II' acceleration reported by Jacques *et al.*[28].

The rate of front advancement was extracted from a sequence of photomicrographs. *Figure 17* shows a schematic representation of the cross-sections indicating two measures of front position scaled by the thickness, s/L and r/L_o. For all three morphologies (*Figure 16*), both measures of scaled front position increase linearly with time$^{1/2}$ until the onset of the shape rearrangement when they have progressed ~75% of the distance to the film centreline; afterwards, the fronts penetrate more slowly until they meet at the centre. The scaled initial rates of front advancement ($[=]\,s^{-0.5}$) match those for the

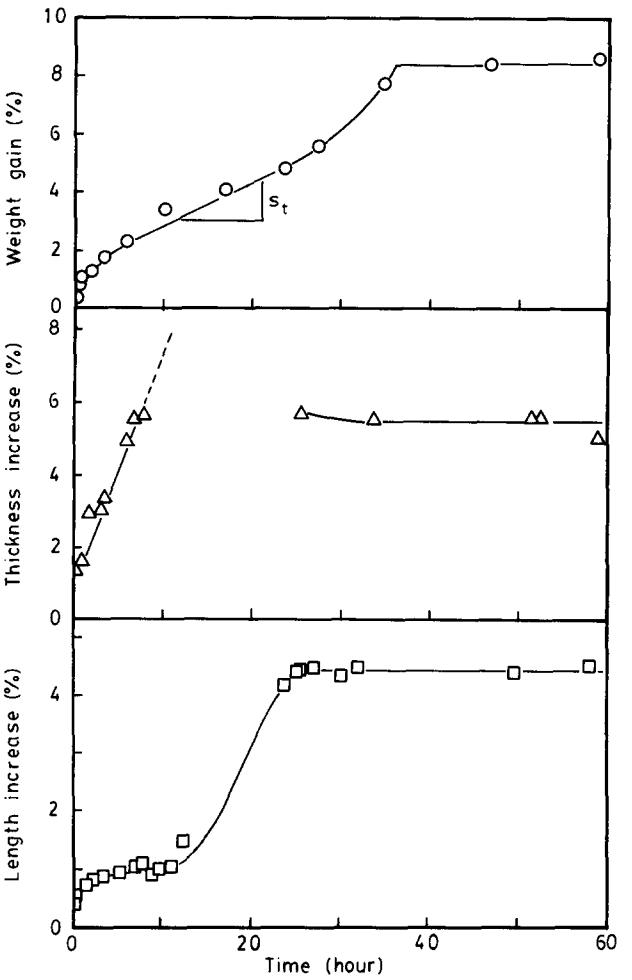

Figure 14 Weight gain and sample dimensional change data *versus* t during acetone sorption at 53°C in films prepared by SINC. The parameter s_t indicates the slope of the Case II region

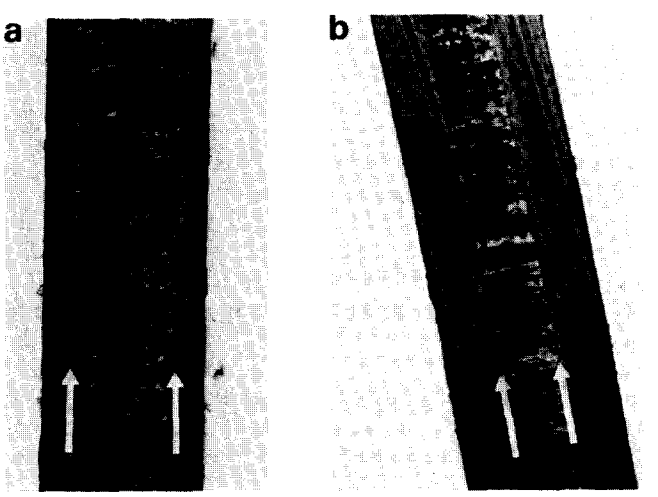

Figure 15 Representative optical micrographs of films prepared by SINC partially swollen with DMF at 65°C. Immersion time: (a) 0.4 h, (b) 1.2 h. Arrows indicate moving boundaries

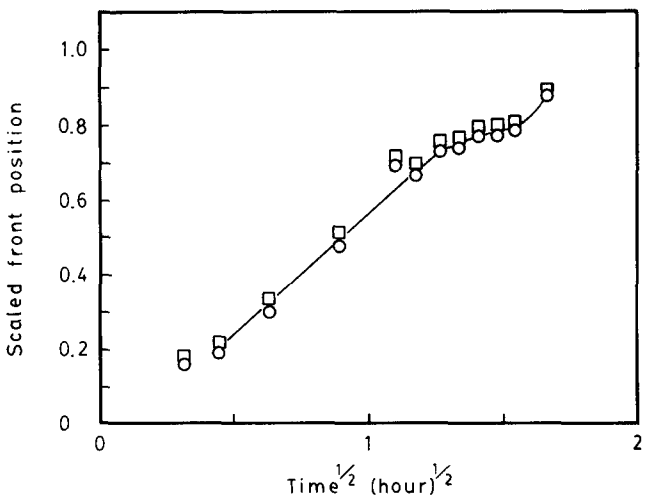

Figure 16 Scaled position of the moving boundary *versus* $t^{1/2}$ during DMF sorption at 65°C in films prepared by SINC; s/L (□), r/L_o (○)

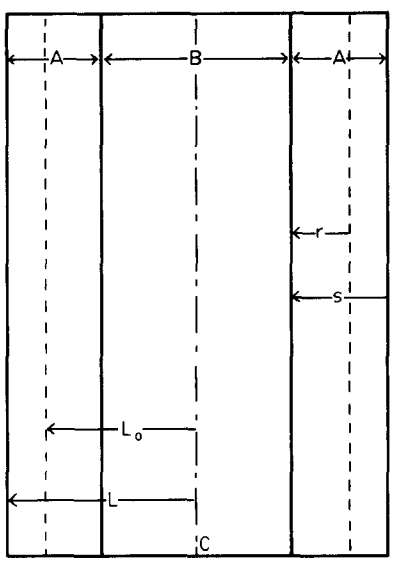

Figure 17 Schematic representation of a cross-section. A, swollen region; B, glassy region; C, film centreline; – – –, original position of the film surfaces. Two measures of scaled front position are defined: s/L, the distance from the current film surface to the front divided by the current film half thickness; r/L_o, the distance from the original film surface to the front divided by the original film half thickness

corresponding weight uptake showing that before the shape rearrangement the weight gain is controlled by the moving boundary motion implying that the region behind the boundary is highly swollen while that in front of the boundary is nearly dry.

Taken together, the data show that DMF transport before the shape rearrangement is consistent with the A&S[9] model in the diffusion controlled limit. A rough estimate of the characteristic distance, l^*, where the rates of swelling and diffusion are equal (Appendix B) supports this as does the desorption data discussed subsequently.

In light of the models, the induction time extracted from the weight gain *versus* $t^{1/2}$ plots (*Figure 12*), t_{ind}, is comprised of the time needed to establish the sharp boundaries at the surface, t_1 (T&W[10]), and for their motion to become diffusion controlled, t_2 (A&S[11]), i.e. $t_{ind} = t_1 + t_2$. Representative data allows us to determine which component is the controlling factor in t_{ind}. *Figure 18* shows the initial portion of the weight gain *versus* time$^{1/2}$ for DMF sorption at 45°C in films prepared by LTA, and indicates the characteristic times just defined; the data show that t_1 (0.19 h) is negligible relative to t_2 (1.25 h). Therefore, we take[9]

$$t_{ind} \simeq t_2 = \frac{D}{U_o^2} \tag{8}$$

for all cases involving DMF. Here U_o is the initial boundary velocity (i.e. $U_o = U_{(t=0)}$). Also, the slope determined from the linear portion of the weight gain *versus* $t^{1/2}$ curve, $s_{\sqrt{t}}$ (*Figure 12*), characterizes diffusion in the swollen region behind the boundary and is proportional to the square root of the penetrant diffusion coefficient, $D^{1/2}$.

Acetone transport. *Figure 14* shows weight gain data plotted against t for acetone sorption at 53°C in PET prepared by SINC. The data for annealed samples and at other temperatures are qualitatively the same. Non-Fickian transport is observed in all cases.

After a short, initial period of rapid absorption linear with $t^{1/2}$, the weight uptake of acetone increases linearly with t (rather than $t^{1/2}$) until ~60% of the total penetrant is absorbed. Afterwards, the slope increases sharply and the equilibrium penetrant uptake is rapidly achieved. The dimensional change data (*Figure 14*) show that this 'Super Case II' acceleration is accompanied by a shape rearrangement as described above for DMF sorption.

The characteristics of acetone sorption before the shape rearrangement can also be understood in terms of the A&S[9] model. Since the weight gain and thickness curves prior to the shape rearrangement are predominantly linear with t, Case II behaviour dominates. An estimate of the characteristic distance, l^*, (Appendix B) shows it to be considerably larger than the film half thickness, L, consistent with the observation of Case II. Accordingly, the slopes, s_t (*Figure 14*), are proportional to the initial front velocity, U_o. The short, initial period of rapid acetone uptake linear with $t^{1/2}$ is best explained by the effect of a significant Fickian

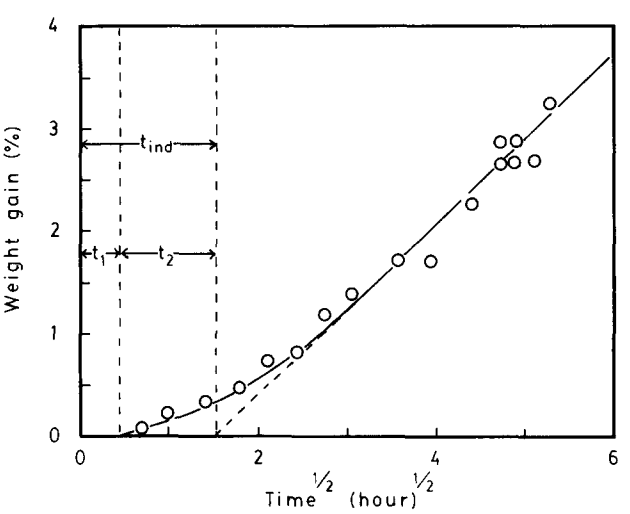

Figure 18 Initial portion of weight gain *versus* $t^{1/2}$ data during DMF sorption at 45°C in films prepared by LTA. The induction time, t_{ind}, the time necessary to establish the fronts, t_1, and the time for diffusion control of the moving boundary, t_2, are indicated

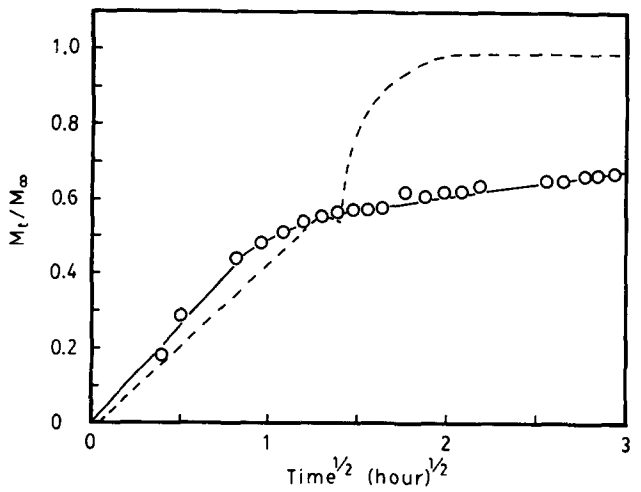

Figure 19 Desorption data at 65°C from films prepared by SINC and swollen to equilibrium with DMF, plotted as $(1-M_t/M_\infty)$ *versus* $t^{1/2}$. ——, Corresponding sorption data

precursor penetrating the glassy polymer ahead of the sharp Case II profiles[11].

Super Case II acceleration. The weight gain data in *Figures 12* and *14* both show 'Super Case II' acceleration first observed by Jacques *et al.*[28] during the integral sorption of n-hexane in very thin films of polystyrene, poly(phenylene oxide), and their blends. This phenomenon was explained[28] by the overlap of Fickian precursors to the Case II concentration profiles accelerating the rate processes controlling their propagation. Other explanations have also been proposed. In their refinement of the A&S model, Gostoli and Sarti[14] attribute the 'Super Case II' effect to an increase in the moving boundary velocity caused by a mechanical stress exerted on the glassy core by the swollen, outer region. Thomas and Windle[24] ascribed the effect to a readjustment of the equilibrium penetrant content after the release of compressive stresses exerted by the glassy core on the swollen region. We observed acceleration in weight uptake during both the diffusion-controlled DMF sorption and the swelling controlled-acetone sorption. In both cases, this increase occurs after the onset of the shape rearrangement, and is accompanied by a slowing of the boundary motion, favouring Thomas and Windle's explanation.

Desorption. Integral desorption supplies additional support for the A&S description of transport prior to shape rearrangements. *Figure 19* shows desorption data at 65°C from films prepared by SINC and swollen to equilibrium in DMF. The plot gives the relative weight loss, $(1-M_t/M_\infty)$, *versus* $t^{1/2}$. The dotted line shows the corresponding sorption data. The data for all three morphologies show common features: the initial rate of desorption is very rapid, and is followed by a much slower rate; the initial desorption is linear with $t^{1/2}$ and exceeds the initial sorption; the sorption and desorption curves intersect.

These characteristics are typical of integral desorption following non-Fickian integral sorption[8] and obey the predictions of the A&S model[13]. In light of this model, the initial desorption being proportional to $t^{1/2}$ reflects that a very thin glassy layer forms immediately at the swollen surface; this remains very thin during most of the process. In effect, desorption occurs by classical diffusion from a swollen film with a very thin, glassy outer shell. The slower secondary rate reflects desorption as the inner swollen region begins to glassify.

Diffusion coefficients for DMF in swollen PET were calculated for each morphology from the initial portion of the desorption curves using a relationship developed by Joshi and Astarita[13]:

$$D=\left[\frac{dw}{dt^{1/2}}\Big/(c^*-c_0)\right]^2 \qquad (9)$$

Here, $dw/dt^{1/2}$ is the initial slope of the $(w_t-w_0)/w_0$ *versus* $t^{1/2}$ curve, where w_t is the sample weight per unit area at time t and w_0 is the initial, dry weight per unit area. The quantity c_0 represents the equilibrium penetrant concentration while c^* is the 'threshold' concentration for swelling[9]. This was estimated using free volume theory[29] as the penetrant concentration depressing the polymer T_g to the experimental temperature. Calculated values of the diffusivity are listed in *Table 5*.

The diffusion coefficients characterize molecular diffusion in the highly swollen semicrystalline material. The values follow the trend in amorphicity: SINC (7.4×10^{-8} cm^2 s^{-1}) > LTA (5.3×10^{-8} cm^2 s^{-1}) > HTA (5×10^{-9} cm^2 s^{-1}).

The desorption data reinforce our earlier conclusion: for acetone and DMF transport in semicrystalline PET, the initial stages of integral sorption and desorption are well described by the A&S[9] model.

Anisotropy of swelling. Dimensional change measurements during the integral sorption of acetone and DMF clearly showed anisotropic swelling in all cases. This usually appears when a sharp boundary accompanies the transport: isotropic volume expansion is not possible because the rigid, glassy core constrains the softened outer layer to swell predominantly in the thickness direction. When the rigid core becomes very thin near the end of sorption, the restraint is removed and a shape rearrangement takes place.

T&W[24] introduced a quantitative index, β, to characterize the departure of the swollen equilibrium state from an isotropic expansion of the initial state:

$$\beta=\frac{\Delta d_\infty/d_0(\Delta d_\infty/d_0+2)}{\Delta A_\infty/A_0} \qquad (10)$$

Here, Δd_∞ is the change in thickness at equilibrium relative to the initial thickness d_0, and ΔA_∞ is the change in area at equilibrium relative to the initial area A_0. A value of $\beta=1$ means an isotropic volume expansion; $\beta>1$ indicates plastic deformation in the thickness direction.

Values of β are given in *Table 6*. For acetone and DMF sorption in SINC and LTA films, significant plastic deformation in the thickness direction ($\beta\simeq1.5$) is observed. For sorption of DMF in films prepared by

Table 5 Diffusion coefficients calculated from DMF desorption data at 65°C

Film preparation	D (cm^2 s^{-1})
SINC	7.4×10^{-8}
Low temperature annealing	5.3×10^{-8}
High temperature annealing	5×10^{-9}

Table 6 Values of anisotropy index β during sorption at different temperatures

Film preparation	DMF 45°C	DMF 65°C	DMF 75°C	Acetone 53°C
SINC	1.45	1.46	1.27	1.25
Low temperature annealing	1.47	1.51	0.95	1.48
High temperature annealing	—	1.13	0.97	—

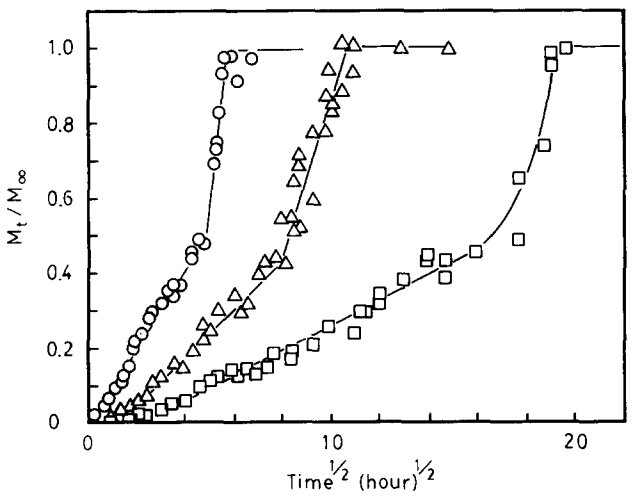

Figure 20 Relative weight uptake, M_t/M_∞, *versus* $t^{1/2}$ during DMF sorption at 45°C in films prepared by SINC (○), LTA (△) and HTA (□)

HTA, where the high crystalline fraction resists swelling and plastic deformation, ΔA_∞ and Δd_∞ were smaller and the expansion was approximately isotropic.

Effect of morphology on non-Fickian transport. The influence of fine structure on the transport of acetone and DMF is quite different than for methanol transport. We showed above that variations in morphology have a rather subtle effect on the methanol transport. By contrast, fine structure strongly affects the DMF transport, while the effect on acetone transport is intermediate.

To illustrate the strong effect of morphology on DMF transport, *Figure 20* shows a plot of relative weight uptake at 45°C *vs.* $t^{1/2}$ for the three different morphologies. All of the curves exhibit similar non-Fickian features, however, the time scales for each are quite different. To quantitatively characterize the effect of morphology, two parameters were extracted from the initial part of the weight gain *versus* $t^{1/2}$ plots: the slope of the initial, linear section, $s_{t^{1/2}}$; and, an induction time, t_{ind}, calculated as the intercept of the linear region with the abscissa from a least squares linear regression. These characterize the transport prior to the shape rearrangement, i.e. during the initial, one-dimensional transport process described by the A&S[9] model.

The initial slopes ($s_{t^{1/2}}$) follow the trend: SINC > LTA > HTA, which parallels the trend in amorphicity. Since $s_{t^{1/2}}$ is proportional to $D^{1/2}$, penetrant diffusion coefficients in the swollen polymer should follow the same trend; this expectation is confirmed for diffusion coefficients obtained from desorption data as discussed above. The decrease in D with α_c can be understood[30] in terms of the increase in diffusion path length with crystallinity as penetrant molecules are forced to circumvent the impenetrable crystallites.

The magnitude of the induction times (t_{ind}) during DMF transport follows the opposite trend: HTA > LTA > SINC, which parallels the trend in crystallinity. As discussed above, the induction time corresponds to the time necessary to establish diffusion control (eq. (8)).

The dependence of the initial front velocity, U_o, on morphology may be understood roughly through the relationship developed by Mills *et al.*[31] from the T&W[10] model:

$$U_o = (D_G \pi_o / \eta_o \phi_1^*)^{1/2} \tag{11}$$

Here, π_o is the maximum osmotic pressure, η_o is the glassy polymer 'viscosity', D_G is the penetrant diffusion coefficient in the glassy polymer ahead of the front, and ϕ_1^* is as defined previously. This leads to an expression for t_{ind}

$$t_{ind} = \frac{D}{D_G} \frac{\eta_o \phi_1^*}{\pi_o} \tag{12}$$

The polymer 'viscosity' (characterizing plastic flow of the dry polymer), η_o, should depend strongly on fine structure, while the other terms should show only slight or negligible dependence; we expect that η_o increases with increasing crystallinity. So, the increase in t_{ind} with α_c seems consistent with the phenomenological models through the influence of α_c on the polymer mechanical properties.

Figure 21 shows a plot of the relative weight uptake *versus* t for the sorption of acetone at 45°C in films with the three different fine structures. The data illustrate the effects found at 35 and 53°C as well. The acetone uptake in SINC films is considerably faster than in the two thermally annealed films which fall on a single curve.

To quantitatively characterize the effect of morphology, slopes of the linear Case II section, s_t (*Figure 14*), were calculated from the initial part of the weight gain *versus* t plots. These follow the trend: SINC > LTA ≈ HTA. The difference between samples prepared by SINC

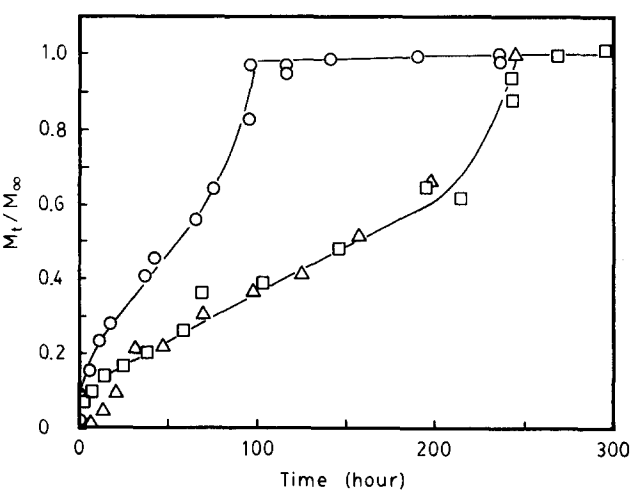

Figure 21 Relative weight uptake, M_t/M_∞, *versus* t during acetone sorption at 45°C in films prepared by SINC (○), LTA (△) and HTA (□)

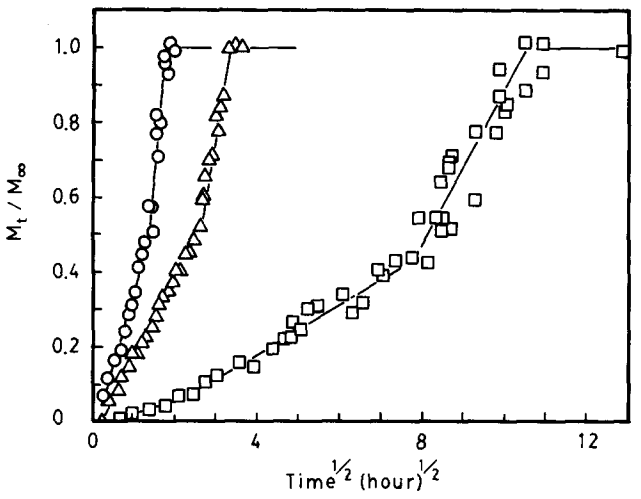

Figure 22 Relative weight uptake, M_t/M_∞, *versus* $t^{1/2}$ during DMF sorption in films prepared by LTA at 45°C (□), 65°C (△) and 75°C (○)

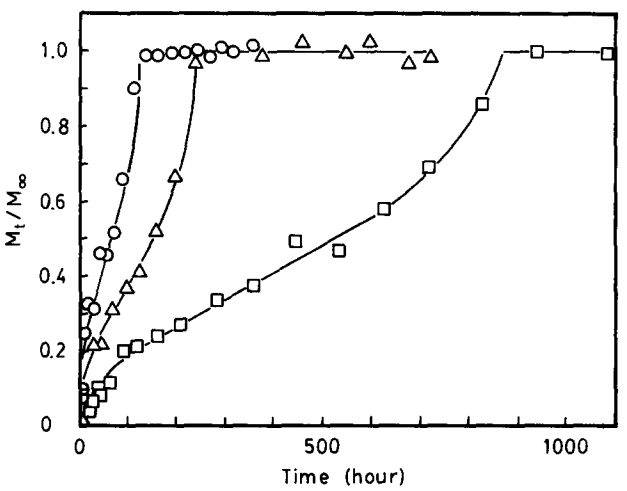

Figure 23 Relative weight uptake, M_t/M_∞, *versus* t during acetone sorption in films prepared by LTA at 35°C (□), 45°C (△) and 53°C (○)

and thermal annealing results from the dependence of U_0 on morphology implied by equation (11). The viscosity η_0 should be considerably lower for solvent crystallized than for thermally prepared samples and probably accounts for the larger front velocity in this case. Curiously, little difference is found between the U_0 for the thermally annealed films although η_0 is presumably larger for films prepared by HTA than LTA. Apparently this difference is balanced by opposite trends in the other terms of equation (11).

Effect of temperature on non-Fickian transport. Figures 22 and *23* show the effect of temperature on the relative weight uptake of DMF and acetone in films prepared by LTA; the trends are representative of those found in SINC and HTA films. No dramatic changes are evident in the character of transport with temperature; only an increase in the rate of each process accompanies increased temperature.

An Arrhenius analysis of $1/t_{ind}$ and $(s_{t^{1/2}})^2$ from the DMF sorption data yields the activation energies, E_{ind} and E_{dif}, respectively (*Table 7*). Similar analysis of s_t from the acetone sorption data gives E_{swel} for the three morphologies (*Table 8*). Due to large uncertainties, trends in the activation energies with morphology are difficult to establish.

As for methanol, we utilize the theory of Pace and Datyner[27] to show that our values of E_{dif} for DMF are consistent with data from the literature[26]. *Figure 24* shows a plot of the predicted activation energy (kJ mol^{-1}) *versus* penetrant diameter (nm) for diffusion in semicrystalline PET above T_g together with our data and that of Michaels *et al.*[26]. The penetrant diameter for DMF (0.68 nm) was calculated from the hard core volume according to Sugden[32] and corrected to a Lennard-Jones diameter at 0°C using a ratio typical for molecules similar in size and geometry to DMF. As in *Figure 11*, the lower curve, calculated using a local chain bending modulus, is applicable for smaller penetrants (He, H_2, O_2) while the upper curve, calculated using a larger averaged bending modulus, is applicable for larger ones. Within the estimated uncertainty of our data, the DMF activation energy data lies on the upper curve.

Table 7 Activation energies for the induction time and for diffusion in the swollen region, E_{ind} and E_{dif}, calculated from DMF sorption data

Film preparation	E_{ind} (kJ mol^{-1})	E_{dif} (kJ mol^{-1})
SINC	+93±35	+113±13
Low temperature annealing	+84±8	+118±20
High temperature annealing	—[a]	—[a]

[a] Characteristic parameters could be extracted from only two data sets so no values are reported

Table 8 Activation energy for front propagation, E_{swel}, calculated from acetone sorption data

Film preparation	E_{swel} (kJ mol^{-1})
SINC	+89±18
Low temperature annealing	+84±16
High temperature annealing	+74±1

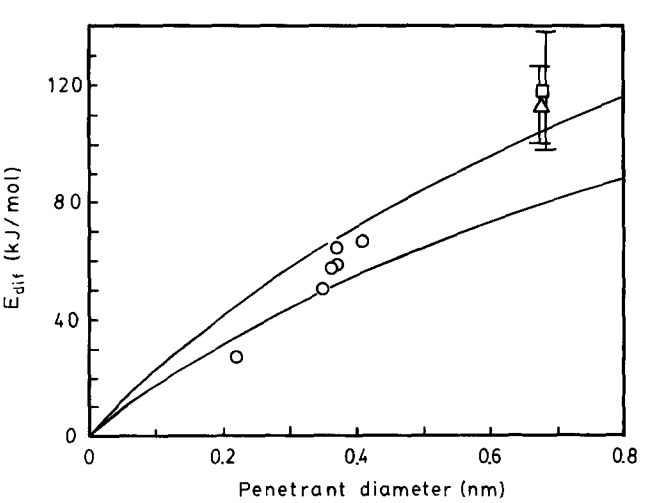

Figure 24 Activation energy for diffusion (kJ mol^{-1}) predicted by the theory of Pace and Datyner[27] *versus* penetrant diameter (nm) for semicrystalline PET above T_g using a local bending modulus (lower curve) and an average bending modulus (upper curve). DMF data with error bars for films prepared by SINC (△) and LTA (□). Data of Michaels *et al.*[26] (○)

Table 9 Activation energy for front propagation, E_{swel}, calculated from DMF sorption data using equation (8)

Film preparation	E_{swel} (kJ mol^{-1})
SINC	+103
Low temperature annealing	+101
High temperature annealing	—

The activation energy for the induction time in DMF, E_{ind}, is slightly smaller than for diffusion, E_{dif}. With equation (8), the activation energy for front propagation in DMF, E_{swel}, can be calculated from E_{ind} and E_{dif} (*Table 9*). The values for PET prepared by SINC and LTA are very near that reported by Haga[33] for the Case II transport of chloroform in oriented, semicrystalline PET ($\sim +100$ kJ mol^{-1}) and slightly larger than values for acetone sorption in SINC and LTA films (*Table 8*).

While from our DMF sorption data E_{dif} is slightly larger than E_{swel}, T&W[10] report a large activation energy for U_o ($+118$ kJ mol^{-1}) and a much smaller value for diffusion ($\sim +59$ kJ mol^{-1}) in the system PMMA/methanol. This feature ($E_{swel} \leqslant E_{dif}$ in PET) has been reported earlier by Durning *et al.*[34]. It is believed to result from similar chain motions being involved in penetrant jumps (associated with E_{dif}) and plastic flow of PET (associated with E_{swel}).

Application of the Deborah number correlation

As discussed in the introduction, Vrentas *et al.*[1] successfully predicted the type of transport (whether Fickian or non-Fickian) when the concentration interval is small according to the value of the diffusion Deborah number:

$$(\mathrm{DEB})_D \equiv \frac{\text{Characteristic relaxation time}}{\text{Characteristic diffusion time}} = \frac{\tau_n}{\theta_D} \tag{13}$$

For transport with a large concentration interval, $(\mathrm{DEB})_D$ varies as a function of time and position throughout the process. A natural extension of Vrentas and Duda's criterion is to expect anomalous behaviour whenever the local value of $(\mathrm{DEB})_D$ passes through O(1) during the process. As a result, Deborah numbers in the initial and final states should be calculated to predict whether non-classical transport will appear.

An order of magnitude calculation shows clearly that for the initial states employed in this study (dry, glassy PET well below T_g), $(\mathrm{DEB})_D$ is very large for all reasonable definitions of τ_n and all combinations of morphology, penetrant, and temperature studied. For the final states, $(\mathrm{DEB})_D$ depends on the equilibrium penetrant concentration; anomalous transport behaviour should be observed when this value is $\leqslant$O(1).

Vrentas *et al.*[1] defined the characteristic diffusion time:

$$\theta_D = \frac{l^2}{D^*} \tag{14}$$

where l is a characteristic distance and D^* is a diffusion coefficient. We interpret D^* as the polymer fixed frame diffusion coefficient, D, and l as the film half thickness, L. Values of D in the fully swollen polymer were calculated from desorption data for methanol and DMF (*Tables 4* and *5*). For acetone, the approximate value reported by Durning and Russel[35] at 35°C is used ($D = 6 \times 10^{-8}$ cm^2 s^{-1}).

The characteristic rheological relaxation time τ_n was originally defined[1]

$$\tau_n \equiv \lambda = \frac{\int_0^\infty sG(s)\,ds}{\int_0^\infty G(s)\,ds} \tag{15}$$

where G is the shear relaxation modulus. For viscoelastic fluids, the integrals in equation (15) are convergent; λ is the terminal relaxation time characterizing the flow zone of the viscoelastic spectrum; it is not defined for crosslinked, semicrystalline, or other viscoelastic systems that do not exhibit flow.

At present, the correct choice of τ_n for viscoelastic solids is unclear. Durning[3] successfully predicted the non-classical trends observed for linear transport utilizing relaxation times in the transition zone; it seems natural to use these for the present case since they are well defined for solids.

Tensile creep data were measured by Ward[36] for a semicrystalline PET monofilament prepared by annealing at 180°C for 1 h. Although not possessing exactly the same fine structure as our samples, Ward's[36] viscoelastic data should provide reasonable estimates for mean relaxation times at the reference conditions. *Figure 25* shows a master curve of log E' *versus* log ω, reduced to 76.6°C, calculated from this data utilizing an approximate relationship[37]:

$$E'(\omega) \simeq 1/J(t)_{\omega = 1/t} \tag{16}$$

Here, E' is the tensile storage modulus, J is the shear creep compliance, and ω is the frequency. Letting $\tau = 1/\omega$, we can identify three reference relaxation times on *Figure 25* corresponding to the onset ($\tau_o^\circ = 10$ s), the middle ($\tau_m^\circ = 3 \times 10^6$ s), and the end ($\tau_e^\circ = 1 \times 10^{12}$ s) of the transition zone.

The reference relaxation times identified above are for the pure polymer reduced to 76.6°C. Ward[36] found the WLF equation[38] with universal constants

$$\log a_T = \frac{-17.74(T - T_g)}{51.6 + T - T_g} \tag{17}$$

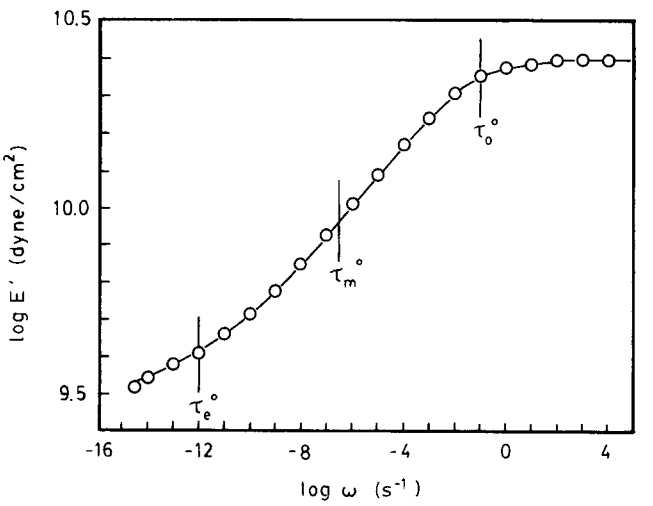

Figure 25 Master curve of log E' (dyne cm^{-2}) *versus* log ω (s^{-1}) reduced to 76.6°C for semicrystalline PET showing the three transition zone relaxation times at the reference condition; from the creep data of Ward[36]

Table 10 Glass transition temperatures for PET films initially and swollen to equilibrium

Film preparation	T_g^o (°C)	ϕ_1^{*a}	T_g^{eff} (°C)[b]
Methanol			
SINC	90	0.082	30
Low temperature annealing	107	0.076	57
High temperature annealing	102	0.076	52
Acetone			
SINC	90	0.166	−53
Low temperature annealing	107	0.145	−36
High temperature annealing	102	0.129	−30
DMF			
SINC	90	0.265	−68
Low temperature annealing	107	0.201	−49
High temperature annealing	102	0.152	−24

[a] Temperature for methanol = 62°C, for acetone = 53°C and for DMF = 65°C

[b] T_g^{eff} was determined from correlation developed by Zachmann and Schermann[22] from dynamic mechanical data for methanol, and calculated from the free volume theory of Kelley and Bueche[29] for acetone and DMF

Table 11 Values for $(DEB)_D$ in the final state for each τ_n^o

Film preparation	Methanol	Acetone	DMF
$\tau_o^o = 10$ s			
SINC	7.0×10^{-12}	7.1×10^{-16}	1.4×10^{-16}
Low temperature annealing	2.9×10^{-7}	2.2×10^{-15}	3.2×10^{-16}
High temperature annealing	1.4×10^{-8}	4.3×10^{-15}	3.1×10^{-16}
$\tau_m^o = 3 \times 10^6$ s			
SINC	2.1×10^{-6}	2.1×10^{-10}	4.1×10^{-11}
Low temperature annealing	8.7×10^{-2}	6.5×10^{-10}	9.7×10^{-11}
High temperature annealing	4.3×10^{-3}	1.3×10^{-9}	9.3×10^{-11}
$\tau_e^o = 10^{12}$ s			
SINC	7.0×10^{-1}	7.1×10^{-5}	1.4×10^{-5}
Low temperature annealing	2.9×10^{4}	2.2×10^{-4}	3.2×10^{-5}
High temperature annealing	1.4×10^{3}	4.3×10^{-4}	3.1×10^{-5}

valid for temperature shifting in the transition region for semicrystalline PET. In order to shift τ_n^o to the temperatures and (amorphous) penetrant volume fractions corresponding to final equilibrium states in our work, we utilize the WLF equation with an effective glass transition temperature for the polymer, T_g^{eff}:

$$\tau_n(T, \phi_1^*) = a_{TC}(T, T_g^{eff})\tau_n^o \quad (18)$$

as suggested by Ferry[39].

Values of T_g for dry PET, determined from the dynamic mechanical data of Illers and Breuer[21] and Zachmann and Schermann[22], appear in *Table 1* for each morphology. These were corrected to the T_g^{eff} for PET-methanol mixtures at equilibrium using an empirical correlation developed by Zachmann and Schermann[22]. For PET–acetone and PET–DMF mixtures, values of T_g^{eff} were roughly estimated using free volume theory[29]. *Table 10* summarizes the results. The equilibrium state values of $(DEB)_D$ calculated from

$$(DEB)_D = \frac{a_{TC}(T, T_g^{eff})\tau_n^o D}{L^2} \quad (19)$$

using each of the τ_n^o in *Figure 25* appear in *Table 11*.

With τ_o^o and τ_m^o, values for $(DEB)_D$ in the final state are all substantially below O(1). Accordingly, anomalous behaviour should appear in all cases. The experimental data, however, contradict this since the sorption of methanol is classical for films prepared by LTA and HTA. This contradiction is resolved if one uses the longest relaxation time in the transition region, τ_e^o. With τ_e^o, $(DEB)_D$ in the final state for methanol remains large for the thermally annealed PET, but is ~O(1) for films prepared by SINC. For acetone and DMF, $(DEB)_D$ in the final state is still well below O(1) regardless of the film's fine structure which agrees with the observation of non-Fickian transport in all cases for these two penetrants.

SUMMARY AND CONCLUSIONS

The transport of methanol, acetone, and DMF in semicrystalline PET spans the range from classical, Fickian to highly anomalous (*Table 12*). The sorption of methanol in PET films prepared by thermal annealing was classical, but for films prepared by SINC, subtle non-Fickian behaviour appeared characterized by anomalous, sigmoid-shaped weight uptake curves. The sorption of acetone and DMF was extremely non-Fickian for all three crystalline fine structures. Here, the initial, one-dimensional transport is consistent with the phenomenological model of A&S[9], but 'Super Case II' acceleration is seen associated with a shape rearrangement just before the moving boundaries reach the centre of the film.

The data reveal that the influence of crystalline fine structure on transport in semicrystalline PET depends on the strength of the swelling agent. For the strong swelling agents, acetone and DMF, the process is non-Fickian and the transport and polymer deformation mechanics are intimately connected. As a result, the change in mechanical properties with morphology strongly influences the rate of transport. For the weak swelling agent, methanol, the transport is basically classical and the process is nearly independent of the polymer mechanical properties, so, the influence of morphology is subtle. The trends with morphology in the non-Fickian process were successfully explained in terms of the T&W model[10,31] for the Case II process.

Table 12 Summary of observed transport behaviour for all three penetrants

Film preparation	Methanol	Acetone	DMF
SINC	Mildly non-Fickian	Non-Fickian, swelling controlled	Non-Fickian, diffusion controlled
Low temperature annealing	Classical	Non-Fickian, swelling controlled	Non-Fickian, diffusion controlled
High temperature annealing	Classical	Non-Fickian, swelling controlled	Non-Fickian, diffusion controlled

Taken together, the transport data for methanol, acetone, and DMF show that as the concentration interval increases, non-classical behaviour becomes dominant. The appearance of anomalous behaviour can be predicted by a suitable extension of the Deborah number correlation. For a substantial concentration interval, one needs to calculate the Deborah number in the initial and final states; anomalous behaviour should occur if the value passes through O(1) during the process. The Deborah numbers clearly predict the experimental trends when the longest relaxation time in the transition zone is chosen as the characteristic rheological time:

$$\tau_1 = \frac{\int_{-\infty}^{+\infty} \tau H(\tau)\, \mathrm{d} \ln \tau}{\int_{-\infty}^{+\infty} H(\tau)\, \mathrm{d} \ln \tau} \tag{20}$$

where $H(\tau)$ is the spectrum of relaxation times.

ACKNOWLEDGEMENTS

The authors gratefully acknowledge the financial support of the National Science Foundation (Grants CPE-84-04263 and CBT-86-17369). Assistance with experimental measurements was provided by Ms E. Chen, Mr F. Wan and Mr P. Portugues.

REFERENCES

1 Vrentas, J. S., Jarzebski, C. M. and Duda, J. L. *AIChE J.* 1975, **21**, 94
2 Vrentas, J. S., Duda, J. L. and Hou, A. C. *J. Appl. Polym. Sci.* 1984, **29**, 399
3 Durning, C. J. *J. Polym. Sci. Polym., Phys. Edn.* 1985, **23**, 1831
4 Vrentas, J. S., Duda, J. L., Ju, S. T. and Ni, L. W. *J. Membr. Sci.* 1984, **18**, 181
5 Durning, C. J. and Tabor, M. *Macromolecules* 1986, **19**, 2220
6 Neogi, P. *AIChE J.* 1983, **29**, 829
7 Alfrey, T., Gurnee, E. F. and Lloyd, W. G. *J. Polym. Sci. (C)* 1966, **12**, 249
8 Fujita, H. *Fortsch. Hoch. Polym. Forsch.* 1964, **3**, 1
9 Astarita, G. and Sarti, G. C. *Polym. Eng. Sci.* 1978, **18**, 388
10 Thomas, N. L. and Windle, A. H. *Polymer* 1982, **23**, 529
11 Astarita, G. and Joshi, S. *J. Membr. Sci.* 1978, **4**, 165
12 Sarti, G. C. *Polymer* 1979, **20**, 827
13 Joshi, S. and Astarita, G. *Polymer* 1979, **20**, 1217
14 Gostoli, C. and Sarti, G. C. *Polym. Eng. Sci.* 1982, **22**, 1018
15 Gibbs, J. W. 'Collected Works', Yale University Press, New Haven, 1948
16 Thomas, N. L. and Windle, A. H. *Polymer* 1978, **19**, 255
17 Durning, C. J., Rebenfeld, L., Russel, W. B. and Weigmann, H. D. *J. Polym. Sci., Polym. Phys. Edn.* 1986, **24**, 1341
18 Dumbleton, J. H. and Murayama, T. *Kolloid-Z. Z. Polym.* 1967, **220**, 41
19 Makarewicz, P. J. and Wilkes, G. L. *J. Polym. Sci., Polym. Phys. Edn.* 1978, **16**, 1559
20 Lin, S. B. and Koenig, J. L. *J. Polym. Sci., Polym. Phys. Edn.* 1982, **20**, 2277
21 Illers, K. H. and Breuer, H. *J. Coll. Sci.* 1963, **18**, 1
22 Zachmann, H. G. and Schermann, W. *Kolloid-Z. Z. Polym.* 1970, **241**, 916
23 Prausnitz, J. M. 'Molecular Thermodynamics of Fluid-Phase Equilibria', Prentice-Hall, Englewood Cliffs, 1969, p. 362
24 Thomas, N. L. and Windle, A. H. *Polymer* 1981, **22**, 627
25 Crank, J. and Park, G. S. 'Diffusion in Polymers' (Eds J. Crank and G. S. Park), Academic Press, London, 1968, Ch. 1
26 Michaels, A. S., Vieth, W. R. and Barrie, J. A. *J. Appl. Phys.* 1963, **34**, 13
27 Pace, R. J. and Datyner, A. *J. Polym. Sci., Polym. Phys. Edn.* 1979, **17**, 453
28 Jacques, C. H. M., Hopfenberg, H. B. and Stannett, V. 'Permeability of Plastic Films and Coatings' (Ed. H. B. Hopfenberg), Plenum Press, New York, 1974, p. 73
29 Kelley, F. N. and Bueche, F. *J. Polym. Sci.* 1961, **50**, 549
30 Peterlin, A. *J. Macromol. Sci. Phys.* 1975, **B11**(1), 57
31 Mills, P. J., Palstrom, C. J. and Kramer, E. J. *J. Mater. Sci.* 1986, **21**, 1479
32 Sugden, S. *J. Chem. Soc.* 1927, 1786
33 Haga, T. *J. Appl. Polym. Sci.* 1981, **26**, 2649
34 Durning, C. J., Rebenfeld, L. and Russel, W. B. *Polym. Eng. Sci.* 1986, **26**, 1066
35 Durning, C. J. and Russel, W. B. *Polymer* 1985, **26**, 131
36 Ward, I. M. *Polymer* 1964, **5**, 59
37 Pinnock, P. R. and Ward, I. M. *Polymer* 1966, **7**, 255
38 Williams, M. L., Landell, R. F. and Ferry, J. D. *J. Am. Chem. Soc.* 1955, **77**, 3701
39 Ferry, J. D. 'Viscoelastic Properties of Polymers', 3rd edn, J. Wiley and Sons, New York, 1980, p. 487

APPENDIX A

A_0 initial sample area
ΔA_∞ change in area at equilibrium relative to A_0
a_T shift factor for temperature defined by equation (17)
a_{TC} temperature–concentration shift factor
c_0 penetrant concentration at equilibrium
c^* critical penetrant concentration for swelling
D penetrant diffusion coefficient in swollen region
d_0 initial sample thickness
Δd_∞ change in thickness at equilibrium relative to d_0
D^* characteristic diffusion coefficient
$(DEB)_D$ diffusion Deborah number
D_G penetrant diffusion coefficient in glassy region
D_T concentration dependent thermodynamic diffusion coefficient
E' tensile storage modulus
E_{dif} activation energy for diffusion in swollen region
E_{ind} activation energy for induction time
E_{swel} activation energy for front propagation
G shear relaxation modulus
G_0 glassy shear relaxation modulus
$H(\tau)$ relaxation spectrum
J shear compliance
J_1 penetrant flux
K empirical constant in equation (1)
k empirical constant in equation (4)
L current film half thickness
l characteristic distance for diffusion
L_0 original film half thickness
l^* characteristic distance where rates of swelling and diffusion are equal
m constant in equation (5)
M_t mass of penetrant absorbed at time t
M_∞ mass of penetrant absorbed at equilibrium
n constant in equation (1) specifying transport behaviour
R gas constant
r distance from the original film surface to the front
s distance from the current film surface to the front
s_t slope of linear region on a weight uptake *versus* t plot
$s_{t^{1/2}}$ slope of linear region on a weight uptake *versus* $t^{1/2}$ plot
T temperature
t time
t_1 induction time associated with front formation
$t_{1/2}$ time for which $M_t/M_\infty = 0.5$
t_2 time necessary for diffusion control of moving boundary

$\tan \delta$ loss tangent
T_g glass transition temperature
T_g^{eff} effective glass transition temperature for polymer–penetrant mixture
t_{ind} induction time on a weight uptake plot
U moving boundary velocity
U_o initial moving boundary velocity (constant with time)
V_1 penetrant molar volume
w_o initial, dry sample weight per unit area
w_t sample weight at time t per unit area
z distance in the lab frame

Greek symbols

α_c crystalline volume fraction
$(1-\alpha_c)$ amorphicity
β anisotropy ratio defined by equation (10)
η concentration dependent polymer viscosity
η_o pure polymer viscosity
θ_D characteristic diffusion time
λ terminal zone relaxation time defined by equation (15)
μ_1 penetrant chemical potential
π osmotic swelling pressure
π_o maximum osmotic swelling pressure
ρ sample density
τ relaxation time
τ_e^o reference relaxation time at end of transition zone
τ_1 longest relaxation time in transition zone
τ_m^o reference relaxation time at middle of transition zone
τ_n characteristic rheological relaxation time
τ_n^o relaxation time at reference conditions
τ_o^o reference relaxation time at onset of transition zone
ϕ_1 ratio of penetrant volume fraction to equilibrium volume fraction at unit activity
ϕ_1^* penetrant volume fraction in amorphous phase
ω frequency

APPENDIX B

In order to assess the rate-determining process in moving boundary type transport, the A&S[9] model defines a characteristic distance, l^*, where the rates of swelling and diffusion are equal:

$$l^* = \frac{D}{U_o} \tag{B1}$$

Here, D is the penetrant diffusion coefficient in the swollen region, while U_o is the initial moving boundary velocity. If $l^* \gg L$, swelling controls the sorption; the sorption is diffusion-controlled if $l^* \ll L$. Evaluation of the characteristic ratio L/l^* for representative experiments allows the determination of the controlling process during DMF and acetone sorption.

In the DMF sorption data at 65 and 75°C, the weight uptake is linear with $t^{1/2}$ from the start; U_o therefore cannot be determined from the data. The data at 25 and 45°C, however, show a short initial region linear with t (*Figure 18*) from which the initial front velocity can be calculated. Although the penetrant concentration behind the front is unknown before the shape rearrangement, if ϕ_1^* is used, the weight gain curve for DMF sorption at 45°C in films prepared by LTA yields the value $U_o \simeq 5 \times 10^{-8}$ cm s^{-1}. The diffusion coefficient at 45°C (3.7×10^{-9} cm^2 s^{-1}) was calculated from the known value (from desorption) at 65°C and the activation energy E_{dif}. For the 0.305 mm thick films employed in DMF sorption, $L/l^* = 0.2$. This indicates that the rates of diffusion and swelling are comparable although the observed transport behaviour suggests it is basically diffusion controlled. Nevertheless, the activation energies for D and U_o indicate that L/l^* should increase with temperature to produce the complete diffusion control observed at higher temperatures.

The initial front velocity during acetone sorption is readily calculated from s_t, the slope of the linear Case II portion of the weight uptake plot (*Figure 14*). If the penetrant content behind the front is assumed equal to ϕ_1^* before the shape rearrangement, the weight gain data during acetone sorption at 45°C in films prepared by SINC gives $U_o \simeq 3 \times 10^{-8}$ cm s^{-1}. When the diffusion coefficient reported by Durning and Russel[35] at 35°C is used (6×10^{-8} cm^2 s^{-1}), $L/l^* = 0.01$ for the 0.406 mm thick films employed. This value indicates that the transport is swelling controlled, in agreement with the experimentally observed behaviour.